Report

Current Biology

The Critical Role of V2 Population Receptive Fields in Visual Orientation Crowding

Highlights

- Crowding effect correlates with the pRF size in V2
- Crowding effect modulates the pRF size in V2
- Perceptual training alleviates crowding and reduces the pRF size in V2

Authors

Dongjun He, Yingying Wang, Fang Fang

Correspondence

ffang@pku.edu.cn

In Brief

He et al. reveal that the pRF size of V2 is closely associated with the orientation crowding effect and suggest the pRFs of V2 as a bottleneck in visual crowding.

He et al., 2019, Current Biology *29*, 2229–2236
July 8, 2019
https://doi.org/10.1016/j.cub.2019.05.068

CellPress

Current Biology
Report

The Critical Role of V2 Population Receptive Fields in Visual Orientation Crowding

Dongjun He,[1,2] Yingying Wang,[2,3,4,5] and Fang Fang[2,3,4,5,6,*]
[1]Sichuan Research Center of Applied Psychology, Chengdu Medical College, Chengdu 610500, China
[2]School of Psychological and Cognitive Sciences and Beijing Key Laboratory of Behavior and Mental Health, Peking University, Beijing 100871, China
[3]Key Laboratory of Machine Perception (Ministry of Education), Peking University, Beijing 100871, China
[4]Peking-Tsinghua Center for Life Sciences, Peking University, Beijing 100871, China
[5]IDG/McGovern Institute for Brain Research, Peking University, Beijing 100871, China
[6]Lead Contact
*Correspondence: ffang@pku.edu.cn
https://doi.org/10.1016/j.cub.2019.05.068

SUMMARY

Crowding, the identification difficulty for a target in the presence of nearby flankers, is an essential bottleneck for object recognition and visual awareness [1, 2]. As suggested by multitudes of behavioral studies, crowding occurs because the visual system lacks the necessary resolution (e.g., small receptive field or high resolution of spatial attention) to isolate the target from flankers and therefore integrates them mistakenly [3–12]. However, this idea has rarely been tested with neuroscience methods directly. Here, using the fMRI-based population receptive field (pRF) technique [13, 14], we found that, across individual subjects, the average pRF size of the voxels in V2 responding to the target could predict the magnitude of visual orientation crowding. The smaller the pRF size, the weaker the crowding effect. Furthermore, we manipulated the magnitude of the crowding effect within subjects. The pRF size in V2 was smaller in a weak crowding condition than in a strong crowding condition, and this difference was attention dependent. More importantly, we found that perceptual training could alleviate the orientation crowding and causally shrink the pRF size in V2. Taken together, these findings provide strong and converging evidence for a critical role of V2 pRFs in visual orientation crowding. We speculate that, synergistic with spatial attention, the dynamic and plastic nature of the V2 pRFs serves to prevent interference from the flankers through adjusting their size and consequently reduces visual crowding.

RESULTS

The population receptive field (pRF) mapping is a widely used technique to measure aggregate human visual receptive field properties by recording non-invasive signals using fMRI. This technique estimates not only the visual field position preferred by each voxel but also its spatial selectivity, the range of visual field locations where a stimulus can evoke a response, indicated by the size of the pRF. We measured the pRFs of the voxels responding to the target in visual cortex (hereafter, these voxels are termed target voxels) and hypothesized that the pRF sizes of the target voxels in some visual area(s) are positively associated with the magnitude of the crowding effect. Our logic is that smaller pRF sizes could help the visual system to isolate and access the target, therefore reducing interference from nearby flankers. We performed a series of psychophysical and fMRI experiments to test this hypothesis. In both the psychophysical and fMRI data analyses, Bonferroni correction was applied with statistical tests involving multiple comparisons.

Experiment 1: Correlation between Crowding Effect and the pRF Size in V2

In all the experiments of this study, the targets and flankers were circular sinusoidal gratings. In experiment 1, the orientation of the target was around 45° or 135°, and the orientations of two flankers were selected between 0° and 180° independently and randomly. We investigated the correlation between the magnitude of the orientation crowding effect and the average pRF size of the target voxels in V1–V4 across individual subjects. In the psychophysical part of experiment 1, as shown in Figure 1A, the target was presented in the upper left visual quadrant, either with two abutting flankers (the flanked condition) or without flankers (the unflanked condition). Using the method of constant stimuli, we measured the orientation discrimination thresholds (75% correct) for the target in these two conditions, which were 8.899° ± 0.766° and 4.425° ± 0.465° (mean ± SEM), respectively. The magnitude of the crowding effect was quantified as the ratio of the discrimination threshold in the flanked condition to that in the unflanked condition—the behavioral crowding index. The index (mean ± SEM: 2.235 ± 0.225) was significantly larger than one (one-sample t test; $t(15) = 5.486$; $p < 0.001$), demonstrating that adding flankers induced a strong crowding effect and impaired orientation discrimination with the target.

In the fMRI part, we used a classical pRF mapping method proposed by Dumoulin and Wandell [13] to estimate the pRF size of the target voxels in V1–V4. During the mapping process, subjects were asked to perform a fixation task while a flickering

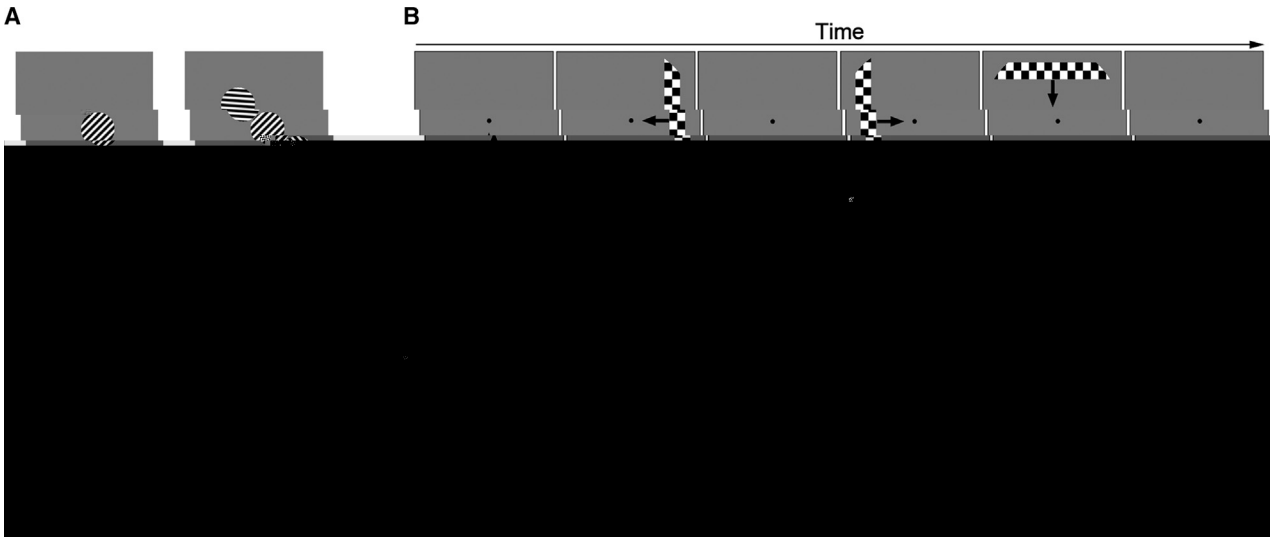

Figure 1. Stimuli, Procedure, and Results of Experiment 1

(A) Unflanked and flanked targets for measuring the magnitude of orientation crowding. The stimuli were presented in the upper left visual quadrant.

(B) pRF mapping procedure. In a stimulus block, a horizontal or vertical checkered bar traversed through a circular aperture. Each run consisted of four stimulus blocks and two blank blocks. The two blank blocks always followed the second and the fourth stimulus block, respectively.

(C) Correlations between the behavioral crowding index and the average pRF size of the target voxels in V1–V4 across individual subjects. Black dot represents the fixation point. Asterisks indicate a statistically significant correlation (**$p < 0.01$).

checkered bar traversed through the visual field (Figure 1B). In other words, the mapping stimulus (i.e., the bar) was irrelevant to the crowding effect. We found that the pRF size of the target voxels increased systematically from V1 to V4 (mean ± SEM; V1, 0.812° ± 0.058°; V2, 1.034° ± 0.086°; V3, 1.540° ± 0.108°; V4, 1.875° ± 0.173°), which is consistent with previous findings [13]. Then we calculated the correlation coefficients between the behavioral crowding index and the average pRF size of the target voxels in each visual area across individual subjects. We found that the correlation was significant in V2 ($r(14) = 0.714$; $p = 0.008$), but not in V1 ($r(14) = 0.576$; $p = 0.078$), V3 ($r(14) = 0.507$; $p = 0.168$), or V4 ($r(14) = 0.395$; $p = 0.427$; Figure 1C). Moreover, the correlation coefficient in V2 was significantly larger than those in V3 ($p = 0.035$) and V4 ($p = 0.005$), but not than that in V1 ($p = 0.099$). These results suggest a close relationship between the magnitude of the orientation crowding effect and the pRF size of the target voxels in V2.

Experiment 2: Attention-Dependent Modulation of the pRF Size in V2 by Crowding Effect

In experiment 1, because the pRF size in V2 and the crowding effect were measured independently and separately, the pRF size variation across subjects might not be ascribed to the crowding effect per se. In experiment 2, we manipulated the magnitude of the orientation crowding effect within subjects and examined whether the crowding magnitude could modulate the average pRF size of the target voxels in V2 and other visual areas. This experiment had two stimulus conditions—the parallel condition and the perpendicular condition, in which the orientation of the flankers was either parallel or perpendicular to that of the target (Figure 2A). Presumably, the parallel condition could elicit a stronger crowding effect than the perpendicular condition because of the similarity of the target and the flankers.

To facilitate the comparison between the psychophysical and fMRI results, the psychophysical part and the fMRI part of experiment 2 were designed similarly. In both parts, instead of presenting the crowding stimuli at a fixed location (as in experiment 1), the target and flankers rotated around the fixation point in steps of 20° every 2 s. Figure 2A shows all the eighteen possible locations where the stimuli were presented. In a 2-s trial, the target and flankers were always presented at one of the eighteen locations and subjects needed to discriminate an 800-ms orientation change of the target (Figure 2B). The target and flankers rotated 20° at the end of each trial. In the psychophysical part, we used the method of constant stimuli to measure the orientation discrimination thresholds (75% correct) for the target in the two stimulus conditions. The threshold in the parallel condition (mean ± SEM: 5.371° ± 0.669°) was significantly higher than that in the perpendicular condition (mean ± SEM: 3.552° ± 0.432°; paired-samples t test; $t(10) = 5.865$; $p < 0.001$). This finding demonstrated that the crowding effect induced by the parallel flankers was stronger than that induced by the perpendicular flankers, confirming the effectiveness of our manipulation.

In the fMRI part, we measured the pRF sizes in V1–V4 when subjects performed the orientation discrimination task with the target of the two stimuli (the attended session) or a demanding fixation task (the unattended session). The orientation changes of the target were always the orientation discrimination thresholds measured in the psychophysical part, ensuring that subjects could perform equally well in the two stimulus conditions. The rotating target and flankers served as the pRF mapping stimulus, which was relevant to the crowding effect in the attended session. The target voxels in experiment 2, as well as in experiments 3 and 4, were defined by the stimulus in Figure 2C, which covered all the areas swept by the rotating target. For each visual

area, we performed a two-way repeated-measures ANOVA with stimulus configuration (parallel versus perpendicular) and attention (attended versus unattended) as within-subject factors (Figure 2D). We found that the main effect of stimulus configuration was significant in V2 ($F_{1,10}$ = 20.252; $p < 0.001$), but not in V1 ($F_{1,10}$ = 1.992; $p = 0.565$), V3 ($F_{1,10}$ = 0.182; $p = 0.989$), or V4

respectively (

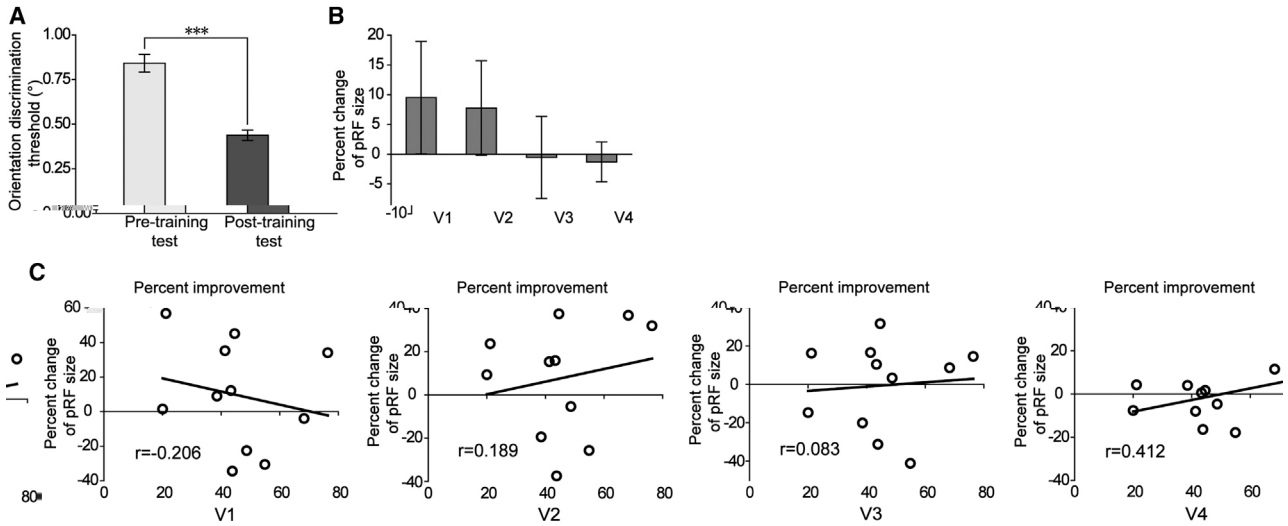

Figure 4. Results of Experiment 4

(A) Orientation discrimination thresholds for the unflanked target in the pre- and post-training tests. Asterisks indicate that subjects' orientation discrimination thresholds after training were significantly smaller than those before training (***$p < 0.001$).

(B) Percent changes of the pRF sizes in V1–V4 from the pre-training test to the post-training test.

(C) Correlations between the percent improvement in orientation discrimination performance with the unflanked target and the percent change of the pRF size in V1–V4. Error bars denote 1 SEM calculated across subjects.

($t(10) = 5.087$; $p < 0.001$), but not in V1 ($t(10) = 0.330$; $p = 0.996$), V3 ($t(10) = 1.570$; $p = 0.471$), or V4 ($t(10) = 0.856$; $p = 0.880$; Figure 3C). In other words, the average pRF size of the target voxels in V2 decreased significantly following the perceptual training. Given that subjects' response accuracies during the pRF mapping were not significantly different between the two test phases (pre-training, 73.727% ± 2.591%; post-training, 73.348% ± 2.622%; paired-samples t test; $t(10) = 0.153$; $p = 0.882$), the observed pRF size change in V2 should not be attributed to differences in task performance and attentional state.

Furthermore, we calculated the correlation coefficients between the behavioral percent improvement and the percent change of the pRF size in V1–V4 across individual subjects. The correlation was significant in V2 ($r(9) = -0.866$; $p < 0.001$), but not in V1 ($r(9) = -0.241$; $p = 0.924$), V3 ($r(9) = -0.483$; $p = 0.432$), or V4 ($r(9) = -0.188$; $p = 0.969$; Figure 3D). Moreover, the correlation coefficient in V2 was significantly larger than those in V1 ($p < 0.001$), V3 ($p < 0.001$), and V4 ($p < 0.001$). The more the reduction of the pRF size in V2, the stronger the learning effect to reduce the orientation crowding. These results provide causal evidence for the critical role of the V2 pRF size in visual crowding.

Experiment 4: Little pRF Size Change after Orientation Discrimination Training with the Unflanked Target

It might be argued that the pRF size reduction observed in experiment 3 was caused by some general perceptual learning effect, rather than the reduction of the crowding effect per se. To examine this issue, we performed experiment 4, which was very similar to experiment 3 except that subjects were trained and tested with the orientation discrimination task with the unflanked target.

After training, subjects' orientation discrimination thresholds decreased significantly (paired-samples t test; $t(10) = 6.489$; $p < 0.001$; Figure 4A). The percent improvement of their behavioral performance was 45.560% ± 5.125% (mean ± SEM), which was significantly larger than zero (one-sample t test; $t(10) = 8.891$; $p < 0.001$) and was comparable to the behavioral learning effect in experiment 3. We failed to find any significant pRF size change in any of the four areas (one-sample t test; V1, $t(10) = 1.009$, $p = 0.807$; V2, $t(10) = 0.976$, $p = 0.824$; V3, $t(10) = 0.078$, $p = 0.999$; V4, $t(10) = 0.389$, $p = 0.992$; Figure 4B). Furthermore, there was no significant correlation between the behavioral percent improvement and the percent change of the pRF size in any of the four areas across individual subjects (V1, $r(9) = -0.206$, $p = 0.956$; V2, $r(9) = 0.189$, $p = 0.968$; V3, $r(9) = 0.083$, $p = 0.999$; V4, $r(9) = 0.412$, $p = 0.607$; Figure 4C). These results suggest that the pRF size reduction in V2 after training is associated with the reduction of the crowding effect rather than a general perceptual learning effect.

DISCUSSION

Using the non-invasive fMRI-based pRF technique in combination with psychophysics, our study has the following major findings. First, even when the magnitude of the orientation crowding effect and the average pRF size of the target voxels in V2 were measured independently, they were positively correlated across subjects. Second, the average pRF size of the target voxels in V2 in the strong crowding condition was larger than that in the weak crowding condition. Third, perceptual training improved subjects' orientation discrimination performance with the crowded target. Meanwhile, it reduced the average pRF size of the target voxels in V2. These two changes were remarkably correlated. Taken together, these findings provide consistent evidence that the orientation crowding effect is closely associated with the average pRF size of the target voxels in V2—the smaller

the pRF, the weaker the crowding effect. Meanwhile, it is noteworthy that V1 exhibited marginally significant effects in experiments 1 and 2, suggesting that V1 pRFs might also contribute to the orientation crowding.

Our study attempts to address the long-standing and central question in visual crowding—the ''bottleneck'' question. Crowding is usually attributed to inappropriate integration or pooling of the target and its flankers over space because peripheral vision lacks sufficient spatial resolution to discern the target and flankers [7, 19]. For example, the receptive field (RF) theory argues that crowding reflects pooling of the target and flankers by receptive fields and therefore occurs when they fall within a single receptive field [3]. When faced with a crowded stimulus, the visual system needs to segment the target and flankers and then individuate and access the target. Therefore, smaller neuronal receptive fields or population receptive fields that cover the target provide a feasible and straightforward way to ensure a weaker crowding effect by reducing inappropriate integration of signals from the target and the flankers. In our study, for the target voxels, some of them responded only to the target. The others responded to both the target and one of the two flankers—their pRFs covered parts of the target and a flanker. We speculate that these pRFs might play a more important role in the crowding effect. For example, the training-induced pRF reduction might allow these voxels to only respond to the target and help to alleviate the crowding effect.

Crowding arises not only when the target and flankers fall within a single classical receptive field but also within a non-classical receptive field [20, 21]. Going beyond the classical receptive field (RF) theory, Sun et al. [22] used ideal observer analysis and a training paradigm to identify the functional mechanism of crowding. They suggest that the mechanism underlying the reduction of crowding following training is attributable to the perceptual window being more capable of adjusting its size to gather relevant information from the target. After training, subjects with inappropriately large windows reduced their window size to exclude interference from flankers. The notion of the perceptual window is similar to what Pelli et al. [19, 23] referred to as ''isolation field'' or ''combination field.'' Our findings here are consistent with Sun et al.'s study and provide the first piece of neuroscience evidence for these ideas.

Our findings are of unique significance in several aspects, both technically and conceptually. First, recent studies started to

metamer. In their model, the first stage decomposes an image with a population of oriented V1-like receptive fields. The second stage computes averages of nonlinear combinations of these responses over regions that scale in size linearly with eccentricity, according to a scaling constant that can be varied parametrically. Given a photographic image, the authors synthesized distinct images with identical model responses and asked whether human observers could discriminate them. From these behavioral data, they estimated the scaling constant that yields metameric images and found that it was consistent with receptive field sizes in V2, suggesting a functional role of this area in information pooling in the periphery. Interestingly, this model can predict degradations of peripheral recognition (i.e., crowding) as a function of both spacing and eccentricity.

Although both the modeling work and our experimental data point to a key role of V2 in orientation crowding, the bottleneck of visual crowding could also exist in other brain areas and networks. This is because the current study only tested low-level orientation discrimination with the crowding stimuli. It has been confirmed that crowding occurs at multiple levels in the visual processing hierarchy [40–43]. For example, Louie et al. [41] demonstrated a holistic crowding between high-level face representations, suggesting that face-selective areas might play a role in this kind of crowding. It should also be noted that, together with previous fMRI studies [44, 45], the current study also suggests that spatial attention or attention resolution is a critical component in the bottleneck. The pRF size change manifested only when subjects' attention was allocated to the crowded targets. In the future, it is worthwhile to examine whether and how crowding is determined by the combination of bottlenecks at multiple levels of cortical processing, including intracortical interaction and high-level attention.

STAR★METHODS

Detailed methods are provided in the online version of this paper and include the following:

- KEY RESOURCES TABLE
- LEAD CONTACT AND MATERIALS AVAILABILITY
- EXPERIMENTAL MODEL AND SUBJECT DETAILS
- METHOD DETAILS
  - Apparatus
  - Stimuli and Design
- QUANTIFICATION AND STATISTICAL ANALYSIS
- DATA AND CODE AVAILABILITY

ACKNOWLEDGMENTS

This work was supported by Ministry of Science and Technology (2015CB351800), National Natural Science Foundation of China (31421003, 61527804, 31671168, 61621136008, and 31800965), and Beijing Municipal Science and Technology Commission (Z181100001518002).

AUTHOR CONTRIBUTIONS

D.H. and F.F. designed the experiments. D.H. collected the data. D.H. and F.F. analyzed the data. D.H., Y.W., and F.F. wrote the paper.

DECLARATION OF INTERESTS

The authors declare no competing interests.

Received: September 12, 2018
Revised: March 26, 2019
Accepted: May 28, 2019
Published: June 20, 2019

REFERENCES

1. Levi, D.M. (2008). Crowding–an essential bottleneck for object recognition: a mini-review. Vision Res. *48*, 635–654.
2. Whitney, D., and Levi, D.M. (2011). Visual crowding: a fundamental limit on conscious perception and object recognition. Trends Cogn. Sci. *15*, 160–168.
3. Flom, M.C., Heath, G.G., and Takahashi, E. (1963). Contour interaction and visual resolution: contralateral effects. Science *142*, 979–980.
4. He, S., Cavanagh, P., and Intriligator, J. (1996). Attentional resolution and the locus of visual awareness. Nature *383*, 334–337.
5. He, S., Cavanagh, P., and Intriligator, J. (1997). Attentional resolution. Trends Cogn. Sci. *1*, 115–121.
6. Intriligator, J., and Cavanagh, P. (2001). The spatial resolution of visual attention. Cognit. Psychol. *43*, 171–216.
7. Levi, D.M., Hariharan, S., and Klein, S.A. (2002). Suppressive and facilitatory spatial interactions in peripheral vision: peripheral crowding is neither size invariant nor simple contrast masking. J. Vis. *2*, 167–177.
8. Levi, D.M., Klein, S.A., and Aitsebaomo, A.P. (1985). Vernier acuity, crowding and cortical magnification. Vision Res. *25*, 963–977.
9. Pelli, D.G. (2008). Crowding: a cortical constraint on object recognition. Curr. Opin. Neurobiol. *18*, 445–451.
10. Strasburger, H. (2005). Unfocused spatial attention underlies the crowding effect in indirect form vision. J. Vis. *5*, 1024–1037.
11. Strasburger, H., and Malania, M. (2013). Source confusion is a major cause of crowding. J. Vis. *13*, 24.
12. Parkes, L., Lund, J., Angelucci, A., Solomon, J.A., and Morgan, M. (2001). Compulsory averaging of crowded orientation signals in human vision. Nat. Neurosci. *4*, 739–744.
13. Dumoulin, S.O., and Wandell, B.A. (2008). Population receptive field estimates in human visual cortex. Neuroimage *39*, 647–660.
14. He, D., Mo, C., Wang, Y., and Fang, F. (2015). Position shifts of fMRI-based population receptive fields in human visual cortex induced by Ponzo illusion. Exp. Brain Res. *233*, 3535–3541.
15. Sagi, D. (2011). Perceptual learning in vision research. Vision Res. *51*, 1552–1566.
16. Seitz, A.R. (2017). Perceptual learning. Curr. Biol. *27*, R631–R636.
17. Watanabe, T., and Sasaki, Y. (2015). Perceptual learning: toward a comprehensive theory. Annu. Rev. Psychol. *66*, 197–221.
18. Zhu, Z., Fan, Z., and Fang, F. (2016). Two-stage perceptual learning to break visual crowding. J. Vis. *16*, 16.
19. Pelli, D.G., and Tillman, K.A. (2008). The uncrowded window of object recognition. Nat. Neurosci. *11*, 1129–1135.
20. Polat, U., Mizobe, K., Pettet, M.W., Kasamatsu, T., and Norcia, A.M. (1998). Collinear stimuli regulate visual responses depending on cell's contrast threshold. Nature *391*, 580–584.
21. Polat, U., and Sagi, D. (1993). Lateral interactions between spatial channels: suppression and facilitation revealed by lateral masking experiments. Vision Res. *33*, 993–999.
22. Sun, G.J., Chung, S.T.L., and Tjan, B.S. (2010). Ideal observer analysis of crowding and the reduction of crowding through learning. J. Vis. *10*, 16.
23. Pelli, D.G., Tillman, K.A., Freeman, J., Su, M., Berger, T.D., and Majaj, N.J. (2007). Crowding and eccentricity determine reading rate. J. Vis. *7*, 1–36.

24. Moutsiana, C., de Haas, B., Papageorgiou, A., van Dijk, J.A., Balraj, A., Greenwood, J.A., and Schwarzkopf, D.S. (2016). Cortical idiosyncrasies predict the perception of object size. Nat. Commun. *7*, 12110.
25. Schwarzkopf, D.S., Anderson, E.J., de Haas, B., White, S.J., and Rees, G. (2014). Larger extrastriate population receptive fields in autism spectrum disorders. J. Neurosci. *34*, 2713–2724.
26. Wandell, B.A., and Winawer, J. (2015). Computational neuroimaging and population receptive fields. Trends Cogn. Sci. *19*, 349–357.
27. Anton-Erxleben, K., and Carrasco, M. (2013). Attentional enhancement of spatial resolution: linking behavioural and neurophysiological evidence. Nat. Rev. Neurosci. *14*, 188–200.
28. Moran, J., and Desimone, R. (1985). Selective attention gates visual processing in the extrastriate cortex. Science *229*, 782–784.
29. Sundberg, K.A., Mitchell, J.F., and Reynolds, J.H. (2009). Spatial attention modulates center-surround interactions in macaque visual area v4. Neuron *61*, 952–963.
30. Womelsdorf, T., Anton-Erxleben, K., Pieper, F., and Treue, S. (2006). Dynamic shifts of visual receptive fields in cortical area MT by spatial attention. Nat. Neurosci. *9*, 1156–1160.
31. Sprague, T.C., and Serences, J.T. (2013). Attention modulates spatial priority maps in the human occipital, parietal and frontal cortices. Nat. Neurosci. *16*, 1879–1887.
32. Kay, K.N., Weiner, K.S., and Grill-Spector, K. (2015). Attention reduces spatial uncertainty in human ventral temporal cortex. Curr. Biol. *25*, 595–600.
33. Baseler, H.A., Gouws, A., Haak, K.V., Racey, C., Crossland, M.D., Tufail, A., Rubin, G.S., Cornelissen, F.W., and Morland, A.B. (2011). Large-scale remapping of visual cortex is absent in adult humans with macular degeneration. Nat. Neurosci. *14*, 649–655.
34. Papanikolaou, A., Keliris, G.A., Papageorgiou, T.D., Shao, Y., Krapp, E., Papageorgiou, E., Stingl, K., Bruckmann, A., Schiefer, U., Logothetis, N.K., and Smirnakis, S.M. (2014). Population receptive field analysis of the primary visual cortex complements perimetry in patients with homonymous visual field defects. Proc. Natl. Acad. Sci. USA *111*, E1656–E1665.
35. Dumoulin, S.O., and Knapen, T. (2018). How visual cortical organization is altered by ophthalmologic and neurologic disorders. Annu. Rev. Vis. Sci. *4*, 357–379.
36. Chung, S.T.L., Li, R.W., and Levi, D.M. (2008). Crowding between first- and second-order letters in amblyopia. Vision Res. *48*, 788–798.
37. Chen, N., Cai, P., Zhou, T., Thompson, B., and Fang, F. (2016). Perceptual learning modifies the functional specializations of visual cortical areas. Proc. Natl. Acad. Sci. USA *113*, 5724–5729.
38. Harvey, B.M., and Dumoulin, S.O. (2011). The relationship between cortical magnification factor and population receptive field size in human visual cortex: constancies in cortical architecture. J. Neurosci. *31*, 13604–13612.
39. Freeman, J., and Simoncelli, E.P. (2011). Metamers of the ventral stream. Nat. Neurosci. *14*, 1195–1201.
40. Chicherov, V., Plomp, G., and Herzog, M.H. (2014). Neural correlates of visual crowding. Neuroimage *93*, 23–31.
41. Louie, E.G., Bressler, D.W., and Whitney, D. (2007). Holistic crowding: selective interference between configural representations of faces in crowded scenes. J. Vis. *7*, 1–11.
42. Manassi, M., and Whitney, D. (2018). Multi-level crowding and the paradox of object recognition in clutter. Curr. Biol. *28*, R127–R133.
43. Ronconi, L., Bertoni, S., and Bellacosa Marotti, R. (2016). The neural origins of visual crowding as revealed by event-related potentials and oscillatory dynamics. Cortex *79*, 87–98.
44. Chen, J., He, Y., Zhu, Z., Zhou, T., Peng, Y., Zhang, X., and Fang, F. (2014). Attention-dependent early cortical suppression contributes to crowding. J. Neurosci. *34*, 10465–10474.
45. Fang, F., and He, S. (2008). Crowding alters the spatial distribution of attention modulation in human primary visual cortex. J. Vis. *8*, 1–9.
46. Brainard, D.H. (1997). The psychophysics toolbox. Spat. Vis. *10*, 433–436.
47. Sereno, M.I., Dale, A.M., Reppas, J.B., Kwong, K.K., Belliveau, J.W., Brady, T.J., Rosen, B.R., and Tootell, R.B. (1995). Borders of multiple visual areas in humans revealed by functional magnetic resonance imaging. Science *268*, 889–893.
48. Engel, S.A., Glover, G.H., and Wandell, B.A. (1997). Retinotopic organization in human visual cortex and the spatial precision of functional MRI. Cereb. Cortex *7*, 181–192.
49. Bandettini, P.A., Jesmanowicz, A., Wong, E.C., and Hyde, J.S. (1993). Processing strategies for time-course data sets in functional MRI of the human brain. Magn. Reson. Med. *30*, 161–173.

STAR★METHODS

KEY RESOURCES TABLE

LEAD CONTACT AND MATERIALS AVAILABILITY

Further information and requests for resources and reagents should be directed to and will be fulfilled by the Lead Contact, Fang Fang (ffang@pku.edu.cn).

EXPERIMENTAL MODEL AND SUBJECT DETAILS

There were 16 subjects (9 male) in Experiment 1, 11 subjects (6 male) in Experiment 2, 11 subjects (5 male) in Experiment 3, and 11 subjects (6 male) in Experiment 4. All subjects were right-handed with reported normal or corrected-to-normal vision and had no known neurological or visual disorders. Their ages ranged from 18 to 29. They gave written, informed consent in accordance with the procedures and protocols approved by the human subject review committee of Peking University.

METHOD DETAILS

Apparatus

In the psychophysical experiments, visual stimuli were displayed on an IIYAMA color graphic monitor (model: HM204DT; refresh rate: 85 Hz; spatial resolution: 1024 × 768; size: 22 inch) with a gray background (12.5 cd/m^2) at a viewing distance of 73 cm. A chin rest was used to stabilize subjects' head position. The fMRI experiments were performed on a 3T Siemens Prisma MRI scanner at the Center for MRI Research at Peking University. MRI data were acquired with a 20-channel phase-array head coil. In the scanner, visual stimuli were back-projected via a video projector (refresh rate: 60 Hz; spatial resolution: 1024 × 768) onto a translucent screen placed inside the scanner bore. Subjects viewed the stimuli through a mirror mounted on the head coil. The viewing distance was 73cm. BOLD signals were measured using an echo-planner imaging (EPI) sequence (TE: 30ms; TR: 2000ms; zceIlgl2290Tf40.5420Tsit2759377.6t27594RC

500 ms blank interval. Subjects were asked to maintain fixation on a central black dot throughout the experiment, and make a 2-alternative-forced-choice (2-AFC) judgment of the orientation of the second target relative to the first one (clockwise or counterclockwise). In a block, each of the five θ values was used eight times.

Before measuring pRFs in visual cortex, we defined retinotopic visual areas (V1, V2, V3, and V4) using a standard phase-encoded method developed by Sereno et al. [47] and Engel et al. [48] in which subjects viewed a rotating wedge and an expanding ring that created traveling waves of neural activity in visual cortex. We also performed a block-design run to identify the voxels in the retinotopic areas responding to the target. These voxels are termed target voxels in this study. The run contained twelve stimulus blocks of 12 s, interleaved with twelve blank blocks of 12 s. The stimulus was identical to the target, except that its orientation was randomly selected between 0° and 180°. It was presented at 5Hz in the stimulus blocks.

Voxel-wise pRF parameters were estimated using the method described in Dumoulin and Wandell [13]. Specifically, hemodynamic response function (HRF) was measured for each subject in a separate run. This run contained 12 trials. In each trial, a flickering full contrast checkered disk with a radius of 10° was presented for 2 s, followed by a 30 s blank interval. The HRF was estimated by fitting the convolution of a 6-parameter double-gamma function with a 2 s boxcar function to the BOLD response elicited by the disk.

Four pRF mapping runs were performed in which a flickering full contrast checkered bar (2° in width) traversed through a circular aperture with a radius of 10° around fixation (i.e., the mapped visual area) (Figure 1B). The bar moved through two orientations (vertical and horizontal) in two opposite directions, resulting in a total of four different stimulus configurations. Each run contained four stimulus blocks of 34 s, one for each stimulus configuration, and two blank blocks of 34 s. In a run, the order of the four stimulus configurations was randomized, but the two blank blocks always followed the second and the fourth stimulus blocks, respectively. In a stimulus block, the bar traversed through the mapped visual area in 17 steps of 1.125° within 34 s. Throughout these runs, subjects performed a color discrimination task at fixation to maintain fixation and control attention.

Experiment 2

This experiment had two stimulus conditions – the parallel condition and the perpendicular condition (Figure 2A). In both conditions, the target was centered at 6.25° eccentricity with two abutting flankers positioned radially. The target and flankers rotated around the fixation point. At the starting position as shown in Figure 2A, the orientation of the target was 45°, either left or right tilted. In the parallel condition, the flankers were parallel to the target. In the perpendicular condition, the flankers were perpendicular to the target. The former condition presumably elicited a stronger crowding effect than the later condition.

In the psychophysical part of Experiment 2, we used the method of constant stimuli to measure orientation discrimination thresholds (75% correct) for the target in the parallel and perpendicular conditions. Each condition had five runs of 270 s. Each run contained five stimulus blocks of 36 s, interleaved with five blank blocks of 18 s (Figure 2B). A stimulus block consisted of eighteen discrimination trials of 2 s. In a discrimination trial, the target and flankers were always presented at one of the eighteen possible locations as shown in Figure 2A and the orientation of the target was changed by α° (α: 1, 3, 5, 7, 9) between 400 and 1200 ms after the onset of the trial, either clockwise or counterclockwise. Subjects were asked to maintain fixation and made a 2-AFC judgment of the direction of the orientation change. The target and flankers rotated 20° around the fixation point at the end of each trial. Only one of the five α values was used in a stimulus block.

In the fMRI part of Experiment 2, we estimated pRF parameters when subjects performed the orientation discrimination task in the two stimulus conditions. The stimuli were identical to those in the psychophysical part except that a rapid serial visual presentation (RSVP) of letters was added at fixation. The fMRI part had two sessions: the attended session and the unattended session. In the attended session, the procedure was similar to that of the psychophysical part, except that the orientation change of the target was always the measured discrimination threshold for each stimulus condition. There were three functional runs of 270 s in each stimulus condition. The unattended session was identical to the attended session, except that subjects performed a very demanding RSVP task at fixation in the stimulus blocks, rather than the orientation discrimination task with the target. In the RSVP task, subjects were asked to detect two targets (X and Y) in a stream of distractors (Z, L, N, and T). Each letter subtended 0.27° of visual angles and was presented for 0.2 s.

In Experiment 2, the same procedures as those in Experiment 1 were used to estimate the HRF and to define V1-V4 and target voxels. The only difference was that the stimulus used for defining target voxels consisted of eighteen gratings that had the same physical parameters as the target in the fMRI part (Figure 2C). The region occupied by the stimulus was exactly the area swept by the rotating target in this experiment.

Experiment 3

This perceptual learning experiment consisted of three phases (Figure 3A): pre-training test (days 1-2), orientation discrimination training (days 3-7), and post-training test (days 8-9). For all the three phases, the visual stimulus (only the parallel stimulus was used), task, and procedures in the psychophysical and fMRI parts were similar to those in the attended session of Experiment 2. The fMRI runs for estimating the HRF and defining V1-V4 and target voxels in Experiment 3 were the same as those in Experiment 2.

During the two test phases, we first measured the orientation discrimination thresholds (75% correct) with the target on days 1 and 8, respectively. The fMRI part was conducted on days 2 and 9 to estimate the pRF parameters of the target voxels, respectively. The measured thresholds on days 1 and 8 were used as the orientation change of the target (i.e., α°) in the fMRI part on days 2 and 9, respectively.

During the training phase, each subject underwent five daily training sessions outside the MRI scanner. Each daily session consisted of eighteen runs – thirteen training runs and five threshold estimation runs. The training runs were similar to those in the fMRI part, except that a high-pitched tone was provided after an incorrect response. In the training runs, the orientation change

of the target was the orientation discrimination threshold that was measured in the five threshold estimation runs on the immediately preceding day. The threshold estimation runs were identical to those in the psychophysical part of the two test phases.

Experiment 4

The procedure and design of Experiment 4 were similar to those of Experiment 3, except that the target were presented without flankers.

QUANTIFICATION AND STATISTICAL ANALYSIS

To estimate the orientation discrimination thresholds, for each condition and subject, data from all runs were pooled together for analysis. The percentage of trials in which subjects made a correct response was plotted as a psychometric function of θ or α. We used a cumulative normal function to fit the psychometric values and interpolated the data to find the 75% accuracy point (i.e., the orientation discrimination threshold).

MRI data were processed using BrainVoyager QX (Brain Innovations, Maastricht, the Netherlands) and custom scripts in MATLAB (Mathworks). The anatomical volume in the retinotopic mapping session was transformed into the Talairach space and then inflated using BrainVoyager QX. Functional volumes in all sessions were preprocessed, including 3D motion correction, linear trend removal, and high-pass filtering (cut-off frequency: 0.015 Hz) using BrainVoyager QX. No subject exhibited excessive head movement (< 2mm in translation, $< 0.5^{\circ}$ in rotation) within any fMRI session. The functional volumes were then aligned to the anatomical volume in the retinotopic mapping session and transformed into the Talairach space. The first 6 s of BOLD signals were discarded to minimize transient magnetic saturation effects.

A general linear model (GLM) procedure was used to define target voxels. Target voxels in V1-V4 were defined as those voxels that responded more strongly to the stimulus than the blank screen ($p < 10^{-3}$, uncorrected) in the localizer run. We estimated pRF parameters for each target voxel using the method proposed by Dumoulin and Wandell [13]. The predicted BOLD signal was calculated from the known visual stimulus parameters, the HRF, and a model of the joint receptive field of the underlying neuronal population. This model consisted of a two-dimensional Gaussian pRF with parameters x_0, y_0, and σ, where x_0 and y_0 are the coordinates of the center of the receptive field, and σ indicates its spread (standard deviation) or size. All parameters were stimulus-referred, and their units were degrees of visual angle. These parameters were adjusted to obtain the best possible fit of the measured BOLD signal. Only the voxels whose pRF model could explain at least 15% of the variance of the raw data were included for further analyses. Given that the time course of BOLD signal consisted of 102 (Experiment 1) and 135 (Experiments 2, 3, and 4) TRs, this threshold corresponded to a significance level of $p < 0.001$ (uncorrected) [49]. In both the psychophysical and fMRI data analyses, Bonferroni correction was applied with statistical tests involving multiple comparisons.

DATA AND CODE AVAILABILITY

FMRI and behavioral data are available upon request by contacting the Lead Contact, Fang Fang (ffang@pku.edu.cn).